

Transversely stable soliton trains in photonic lattices

Jianke Yang

Department of Mathematics and Statistics, University of Vermont, Burlington, Vermont 05401, USA

(Received 2 June 2011; published 20 September 2011)

We report the existence of transversely stable soliton trains in optics. These stable soliton trains are found in two-dimensional square photonic lattices when they bifurcate from X -symmetry points with saddle-shaped diffraction inside the first Bloch band and their amplitudes are above a certain threshold. We also show that soliton trains with low amplitudes or bifurcated from edges of the first Bloch band (Γ and M points) still suffer transverse instability. These results are obtained in the continuous lattice model and are further corroborated by the discrete model.

DOI: [10.1103/PhysRevA.84.033840](https://doi.org/10.1103/PhysRevA.84.033840)

PACS number(s): 42.65.Tg, 05.45.Yv

I. INTRODUCTION

It is well known that, in homogeneous optical media, a bright soliton stripe, which is localized along the longitudinal direction and uniform along the transverse (stripe) direction, is always unstable to transverse perturbations [1–7]. When the longitudinal and transverse diffractions have the same sign, the instability is of the neck type, which breaks up the stripe into filaments [4,6,7], but when the two diffractions have the opposite sign, the instability is of the snake type, which bends the stripe to a wavy form [5–7]. These two types of instabilities have been experimentally observed as well [3,8]. When a one-dimensional optical lattice is imposed along the longitudinal or transverse direction of the soliton stripe, the soliton stripe is still transversely unstable [9,10]. While the transverse instability can be utilized for certain applications (such as pulse compression), in many other cases (such as experiments in lower dimensions) it is detrimental and undesirable. To suppress this transverse instability, some ideas have been proposed. For instance, this instability can be completely eliminated if the soliton stripe is made sufficiently incoherent along the transverse direction [11]. This instability can also be significantly reduced (but not eliminated) by nonlinearity saturation or incoherent mode coupling [12,13]. Beside optics, the transverse instability is also a common phenomenon in other branches of physics such as water waves [6,14–16].

In this paper, we report the existence of coherent and transversely stable soliton trains in optics. These stable soliton trains are discovered in two-dimensional photonic lattices. They comprise a periodic sequence of intensity lumps along the transverse direction and are localized along the longitudinal direction. These soliton trains, which are exact stationary solutions of the underlying nonlinear lattice system [17–19], are transversely stable when they bifurcate from the X -symmetry point (with saddle-shaped diffraction) inside the first Bloch band of the lattice their amplitude is above a certain threshold value. This finding is first obtained in the full continuous lattice model. Then it is also corroborated by the discrete nonlinear Schrödinger model, which is shown to support transversely stable discrete line solitons as well under similar conditions. Physically, these soliton trains are transversely stable due to the stabilizing effect of the photonic-lattice potential. However, the photonic lattice does not stabilize every soliton train. Specifically, low-amplitude soliton trains as well

as soliton trains that bifurcate from edges of the first Bloch band (Γ and M points) are still transversely unstable. These transversely unstable soliton trains will also be explained both mathematically and physically.

II. SOLITON TRAINS IN TWO-DIMENSIONAL PHOTONIC LATTICES

The theoretical model we use for coherent-beam propagation in a two-dimensional (2D) photonic lattice is [7]

$$iU_z + U_{xx} + U_{yy} + n(x,y)U + \sigma|U|^2U = 0, \quad (2.1)$$

where z is the direction of propagation, (x,y) is the plane orthogonal to the propagation direction, $n(x,y)$ is the periodic refractive-index variation on the orthogonal plane, and $\sigma = \pm 1$ represents the self-focusing and self-defocusing nonlinearity, respectively. All variables have been normalized. In our analysis, we take the lattice to be

$$n(x,y) = h(\cos^2 x + \cos^2 y), \quad (2.2)$$

where h is the index-variation depth parameter. This is a square lattice which arises frequently in optics and in Bose-Einstein condensates [7,20]. This lattice is π periodic along both x and y directions and is displayed in Fig. 1(a). Below, x and y will be called the principal axes of the lattice since, along them, the lattice has the smallest period. This lattice supports soliton trains aligned along various directions in the (x,y) plane [17–19]. In this paper, we only consider soliton trains aligned along a principal axis of the lattice for simplicity and take this principal axis to be the y direction. Such soliton trains are of the form

$$U(x,y,z) = u(x,y)e^{-i\mu z}, \quad (2.3)$$

where $u(x,y)$ is a real-valued function which is localized along the longitudinal x direction and periodic along the transverse y direction, and μ is the propagation constant. The function $u(x,y)$ satisfies the equation

$$u_{xx} + u_{yy} + \mu u + n(x,y)u + \sigma u^3 = 0. \quad (2.4)$$

In this section, we examine these soliton train solutions.

When $u(x,y)$ is infinitesimal, Eq. (2.4) becomes a linear equation whose bounded solutions are Bloch modes:

$$p(x,y;\mu) = e^{i(k_1x+k_2y)} \hat{p}(x,y;\mu), \quad (2.5)$$

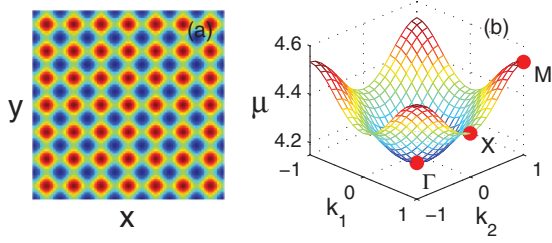


FIG. 1. (Color online) (a) Photonic lattice (2.2) (with $h = 6$). (b) Diffraction surface $\mu = \mu(k_1, k_2)$ of the first Bloch band for this lattice. The high-symmetry points $\Gamma = (0,0)$, $X = (1,0)$, and $M = (1,1)$ in the irreducible Brillouin zone $-1 \leq k_1, k_2 \leq 1$ are marked by red dots.

where $\hat{p}(x, y; \mu)$ is π periodic in both (x, y) , k_1 , and k_2 are wave numbers in the irreducible Brillouin zone $-1 \leq k_1, k_2 \leq 1$, and

$$\mu = \mu(k_1, k_2) \quad (2.6)$$

is the diffraction relation. This diffraction relation can be computed effectively by the Fourier expansion method (see, e.g., Sec. 7.2.3 in Ref. [21]; a MATLAB code for this computation is also available on the author's web page). At the lattice depth $h = 6$, the diffraction function for the first (lowest) Bloch band is shown in Fig. 1(b). If the linear Bloch mode $p(x, y; \mu)$ is required to be real, this mode must then be at one of the high-symmetry points $\Gamma = (0,0)$, $M = (1,1)$, and $X = (1,0)$, $(0,1)$ in the irreducible Brillouin zone and be π or 2π periodic in x and y . For the first Bloch band [see Fig. 1(b)], Γ and M are the lower and upper edge points, respectively, and X lies inside the Bloch band where the diffraction surface has a saddle shape. In this paper, we only consider soliton trains bifurcated from this first band.

When $u(x, y)$ is small but not infinitesimal, Eq. (2.4) is weakly nonlinear, and its solution is a weakly modulated Bloch-wave packet which bifurcates out from the underlying high-symmetry point of the Bloch band. When this solution is a soliton train along the y direction, it can be expanded in a perturbation series

$$u(x, y) = \epsilon A(X)p(x, y) + \epsilon^2 A'(X)v_1(x, y) + \dots, \quad (2.7)$$

$$\mu = \mu_0 + \tau \epsilon^2, \quad (2.8)$$

where μ_0 is the propagation constant of the high-symmetry point, $p(x, y)$ is the Bloch wave at μ_0 , and $v_1(x, y)$ is a generalized Bloch function at μ_0 which satisfies the equation

$$\partial_{xx} v_1 + \partial_{yy} v_1 + [\mu_0 + n(x, y)]v_1 = -2\partial_x p, \quad (2.9)$$

where $\tau = \pm 1$, $0 < \epsilon \ll 1$, $X = \epsilon x$ is the slow spatial variable, and $A(X)$ is the one-dimensional (1D) envelope of this Bloch wave. Notice that the solution $v_1(x, y)$ to Eq. (2.9) is periodic in both x and y with the same period as $p(x, y)$. In addition, this solution is not unique since one may add an arbitrary homogeneous solution $\zeta p(x, y)$, where ζ is a free constant. Returning to the expansion (2.7), we can see that adding $\zeta p(x, y)$ to $v_1(x, y)$ amounts to a shift in the position of

the envelope $A(X)$. In order to fix the location of the envelope $A(X)$, we require that $v_1(x, y)$ be orthogonal to $p(x, y)$:

$$\int_{-\pi}^{\pi} \int_{-\pi}^{\pi} p(x, y)v_1(x, y)dx dy = 0. \quad (2.10)$$

This orthogonality requirement uniquely determines the solution $v_1(x, y)$. In the present case, the lattice $n(x, y)$ in (2.2) is symmetric in x , then $p(x, y)$ is either symmetric or antisymmetric in x . In this case, $v_1(x, y)$ would have the opposite x symmetry of $p(x, y)$ under the above orthogonality condition.

By inserting this perturbation expansion into Eq. (2.4) and following an analysis very similar to [22], we find that the envelope $A(X)$ satisfies the following equation:

$$D_1 A_{XX} + \tau A + \sigma \alpha A^3 = 0, \quad (2.11)$$

where the x direction diffraction coefficient D_1 and the nonlinear coefficient α are given by

$$D_1 = \frac{1}{2} \left. \frac{\partial^2 \mu(k_1, k_2)}{\partial k_1^2} \right|_{\mu=\mu_0}, \quad \alpha = \frac{\int_{-\pi}^{\pi} \int_{-\pi}^{\pi} p^4(x, y)dx dy}{\int_{-\pi}^{\pi} \int_{-\pi}^{\pi} p^2(x, y)dx dy}.$$

When $\text{sgn}(D_1) = \text{sgn}(\sigma) = -\text{sgn}(\tau)$, the envelope equation (2.11) admits a hyperbolic secant soliton:

$$A(X) = \sqrt{\frac{2}{|\alpha|}} \text{sech} \frac{X - X_0}{\sqrt{|D_1|}}, \quad (2.12)$$

where $X_0 = \epsilon x_0$ is the location of the peak of the envelope function $A(X)$. When the Bloch wave $p(x, y)$ is modulated by this 1D hyperbolic secant envelope, the resulting solution (2.7) is then a low-amplitude soliton train along the y direction.

One may notice that the envelope equation (2.11) is translation-invariant, hence X_0 is a free parameter in the envelope solution (2.12). This seems to imply that soliton trains can be obtained regardless of the position of the envelope (2.12) relative to the underlying periodic potential. This is not true, however. In a similar 1D-lattice model, it has been shown that the peak of the envelope can only be located at two positions relative to the lattice [7,23,24]. A slight extension of that analysis to the present 2D soliton train problem shows that the envelope (2.12) of the soliton train, for the symmetric cosine lattice (2.2), must also be located at one of the two positions

$$x_0 = 0, \pi/2. \quad (2.13)$$

The resulting soliton train with $x_0 = 0$ is called the onsite soliton train, and the other one with $x_0 = \pi/2$ is called the offsite soliton train. The offsite train resides at (x, y) regions of low refractive indices $n(x, y)$ and is thus expected to always be unstable [7,23,24]. Thus, we only consider onsite soliton trains in the rest of this article.

When the amplitude of the soliton train is not small, the above perturbation series would be invalid. In such cases, soliton trains can be determined numerically by either the squared-operator iteration methods or the Newton-conjugate-gradient method (see Sec. 7.2 in Ref. [7]). To illustrate, we take self-defocusing nonlinearity ($\sigma = -1$) and lattice depth $h = 6$. In this case, a family of soliton trains bifurcates out from the X point inside the first Bloch band. The quasipower curve

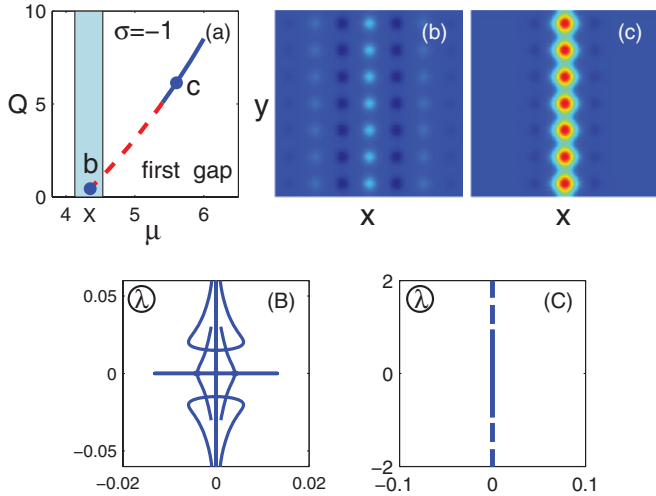


FIG. 2. (Color online) (a) Quasipower curve of soliton trains bifurcated from the X point inside the first Bloch band under defocusing nonlinearity. The dashed (red) segment is transversely unstable, while the solid (blue) segment is stable. Panels (b) and (c) show profiles $u(x,y)$ of soliton trains at low and high amplitudes respectively. These solutions are located at the points marked by the same letters on the quasipower curve of (a). Panels (B) and (C) show linear-stability eigenvalue (λ) spectra in the complex plane for the soliton trains in (b) and (c).

of this family is displayed in Fig. 2(a). Here, the quasipower Q is defined as the integral of u^2 from $-\infty < x < \infty$ and on one transverse period $0 \leq y \leq \pi$; that is,

$$Q = \int_{-\infty}^{\infty} dx \int_0^{\pi} dy u^2(x,y). \quad (2.14)$$

Two typical soliton trains with low and high amplitudes (quasipowers) are displayed in Figs. 2(b) and 2(c), respectively. The propagation constants for these two soliton trains are $\mu = 4.3495$ and 5.6 . One can see that the intensity peaks of these solitons are in phase with each other along the transverse (y) direction, but adjacent intensity peaks along the longitudinal (x) direction are out of phase with each other. In addition, the soliton train near the X point has low amplitude and quasipower and is longitudinally broad (occupying many lattice sites), while that away from the X point has high amplitude and quasipower, and is longitudinally strongly localized (occupying practically a single lattice site). This type of soliton train has been theoretically predicted and experimentally observed in Ref. [19]. In Fig. 4 later in the text, another family of soliton trains bifurcated from the M -symmetry point of the first Bloch band will also be displayed.

In the next section, we will examine the transverse stability of soliton trains. Before detailed analysis, let us first develop some intuition. The soliton trains exist under both self-focusing and self-defocusing nonlinearities ($\sigma = \pm 1$), and they can bifurcate from the Γ and M points at the edges of the Bloch band [17,18] or from X points inside the Bloch band [19]. For soliton trains bifurcated from the Γ point (which occurs under the self-focusing nonlinearity) [17], the intensity peaks along the transverse (train) direction are all in phase. For soliton trains bifurcated from the M point (which occurs under

the self-defocusing nonlinearity) [18], the adjacent intensity peaks along the transverse direction are all out of phase (if this transverse direction is along a principal axis of the lattice as in our present case, see Fig. 4). It is known that in-phase dipoles under the self-focusing nonlinearity and out-of-phase dipoles along a principal axis of the lattice under the self-defocusing nonlinearity are both unstable [7,25–28]. Then, if the soliton trains are strongly localized along the longitudinal direction [which occurs at large amplitudes, see Fig. 4(c)], we may view the soliton trains as a collection of transverse dipoles; hence we may expect soliton trains bifurcated from the Γ and M points to be unstable. However, for soliton trains bifurcated from the X points (under either self-focusing or self-defocusing nonlinearity), adjacent transverse intensity peaks are out of phase under the self-focusing nonlinearity and are in phase under the self-defocusing nonlinearity (see Fig. 2 and Ref. [19]). Dipoles with such phase structures are stable in deep lattices [7,25–28]. Thus, soliton trains bifurcated from X points [at high amplitudes as in Fig. 2(c)] may be free of transverse instabilities. In the next two sections, we will confirm that these intuitions are largely correct; hence transversely stable soliton trains will be discovered.

It should be cautioned, however, that these intuitions are reasonable only when the soliton trains have high amplitudes so that they are strongly longitudinally localized [as in Figs. 2(c) and 4(c)], which makes the transverse-dipole analogy meaningful. If the soliton trains have low amplitude, then they are longitudinally broad and occupying many lattice sites [see Fig. 2(b)]. In that case, longitudinal intersite coupling becomes important, which makes the above transverse-dipole analogy inappropriate. As we will show later, all low-amplitude soliton trains are transversely unstable.

III. TRANSVERSELY STABLE SOLITON TRAINS

In this section, we study the transverse stability of soliton trains in 2D photonic lattices and show that transversely stable soliton trains exist.

First, we briefly show that low-amplitude soliton trains are always transversely unstable. To show this, we consider the dynamics of a low-amplitude soliton train, whose solution can be expanded into a perturbation series

$$U(x,y,z) = e^{-i\mu_0 z} [\epsilon \Psi(X,Y,Z) p(x,y) + \epsilon^2 U_2 + \dots], \quad (3.1)$$

where μ_0 is the propagation constant of a high-symmetry point, $p(x,y)$ is the Bloch wave at μ_0 , $0 < \epsilon \ll 1$, $X = \epsilon x$ and $Y = \epsilon y$ are slow spatial variables, $Z = \epsilon^2 z$ is the slow propagation-distance variable, and $\Psi(X,Y,Z)$ is the envelope function of this low-amplitude soliton train. Following the analysis of Ref. [22], it is easy to show that the evolution of the envelope function $\Psi(X,Y,Z)$ is governed by the following constant-coefficient 2D nonlinear Schrödinger (NLS) equation

$$i \Psi_Z + D_1 \Psi_{XX} + D_2 \Psi_{YY} + \sigma \alpha |\Psi|^2 \Psi = 0, \quad (3.2)$$

where D_2 is the y -direction diffraction coefficient,

$$D_2 = \frac{1}{2} \frac{\partial^2 \mu(k_1, k_2)}{\partial k_2^2} \Big|_{\mu=\mu_0},$$

and D_1 and α have been given before. This 2D envelope equation admits a line-soliton solution:

$$\Psi(X, Y, Z) = A(X)e^{-i\tau Z}, \quad (3.3)$$

where $\tau = -\sigma$ and $A(X)$ is given in Eq. (2.12). This envelope line soliton, when modulated onto the Bloch mode $p(x, y)$, yields the low-amplitude soliton train (2.7) derived in the previous section. It is well known that this envelope line soliton (3.3) is transversely unstable in the constant-coefficient 2D envelope equation (3.2) [1,6,7]. Thus, low-amplitude soliton trains (2.7) are also transversely unstable. Since the transverse instability of low-amplitude soliton trains is induced by the transverse instability of their envelope line solitons, obviously the longitudinal-wave coupling plays an important role in this instability (as has been pointed out at the end of the previous section).

We can further derive the analytical formula for unstable eigenvalues of low-amplitude soliton trains. Since the soliton train is periodic along the transverse direction, the normal modes of infinitesimal disturbances to the train are of the form $\tilde{\Psi} \sim e^{iky+\lambda z}\psi(x, y)$, where k is the transverse wave number of the disturbance, λ is the eigenvalue, and $\psi(x, y)$ is π periodic in y . From the above analysis and after variable scalings, it is easy to show that the eigenvalue $\lambda(k)$ is given by

$$\lambda(k) = \epsilon^2 \Lambda(\sqrt{|D_2|}k/\epsilon), \quad (3.4)$$

where $\Lambda(K)$ is the eigenvalue of the normalized hyperbolic secant line soliton

$$\Phi_0(X, Y, Z) = \sqrt{2} \operatorname{sech} X e^{iZ} \quad (3.5)$$

in the unit-coefficient 2D NLS equation

$$i\Phi_Z + \Phi_{XX} + \operatorname{sgn}(D_1 D_2)\Phi_{YY} + |\Phi|^2\Phi = 0 \quad (3.6)$$

for the disturbance proportional to e^{iKY} , which has been obtained in Refs. [7,29]. A more rigorous derivation of the eigenvalue formula (3.4), which is based on the study of the linear-stability eigenvalue problem of low-amplitude soliton trains, can also be made by a slight modification of the analysis in Ref. [30].

If the low-amplitude soliton train bifurcates from the X -symmetry point (as in Fig. 2), $\operatorname{sgn}(D_1 D_2) = -1$, hence the envelope's transverse instability is of the snake type. Since $D_1 D_2 < 0$, the diffraction surface at the X point has a saddle shape [see Fig. 1(b)]. If the train bifurcates from the edges of the first Bloch band (as in Fig. 4), $\operatorname{sgn}(D_1 D_2) = 1$, hence the envelope's transverse instability is of the neck type.

When the amplitude of the soliton train is not small, the analytical stability analysis above becomes invalid. Below, we numerically investigate the transverse stability of higher-amplitude soliton trains by computing their whole linear-stability spectra using the Fourier collocation method described in Sec. 7.3 of Ref. [7].

First, we consider the soliton trains in Fig. 2, which bifurcate from the X -symmetry point of the first Bloch band. The numerically obtained linear-stability spectra for the low- and high-amplitude soliton trains of Figs. 2(b) and 2(c) are displayed in Figs. 2(B) and 2(C), respectively. The spectrum in Fig. 2(B) contains both real and complex unstable eigenvalues which lie on the right half of the spectral λ plane, indicating

that the low-amplitude soliton train in Fig. 2(b) is transversely unstable. This numerical result agrees with the analytical result given above. Quantitatively we have also compared these numerical eigenvalues with the analytical formula (3.4) and with the function $\Lambda(K)$ provided in [7,29] and found excellent quantitative agreement as well.

A more important finding on this family of soliton trains is that, when the amplitude (or quasipower) of these soliton trains exceeds a certain threshold, transverse instability disappears, and these soliton trains become fully stable. This can be seen in Fig. 2(C), which gives the linear-stability spectrum for the high-amplitude soliton train in Fig. 2(c). This spectrum does not contain any unstable eigenvalue, indicating that this high-amplitude soliton train is fully stable. What happens is that, as μ moves away from the X point $\mu_0 = 4.330$ (i.e., as ϵ increases), the unstable eigenvalues initially increase in size and drift away from the imaginary axis of the spectral plane, as is predicted by the analytical formula (3.4). However, as μ increases further, the unstable eigenvalues turn around and start to move toward the imaginary axis (hence the transverse instability weakens). When $\mu > \mu_c \approx 5.44$, or $Q > 5.3$, all unstable eigenvalues merge into the imaginary axis, hence instability vanishes and the soliton trains become transversely stable. Physically, what happens is that, as μ moves away from the X point, the soliton train transforms from a low-amplitude longitudinally broad train into a high-amplitude longitudinally narrow train [see Figs. 2(b) and 2(c)]. In this process, the snaking instability of the low-amplitude longitudinally broad soliton train is eventually arrested by the lattice when the train becomes strongly localized longitudinally.

We have found that the high-amplitude soliton train in Fig. 2(c) is not only linearly stable, but also nonlinearly stable. To demonstrate its nonlinear stability, we simulate its evolution in Eq. (2.1) when it is initially perturbed by 10% random-noise transverse perturbations. This evolution simulation is performed using the fourth-order split-step method (see Sec. 7.1 of Ref. [7]). After long-distance simulations, we have found that this train remains robust and does not break up at all. For instance, one simulation result (with simulation distance $z = 100$) is displayed in Fig. 3.

The soliton train in Fig. 2(c) may remind us of the train of lumps which form after the onset of the neck-type transverse instability to a line soliton in a homogeneous medium [3,7]. However, it is important to recognize that the train of lumps in a homogeneous medium is not a stable structure. Upon further propagation, it will break up [7]. In contrast, the soliton train in Fig. 2(c) is both linearly and nonlinearly stable and can propagate for all distances without breakup (see Fig. 3). Here, the photonic lattice plays an important role in the stabilization of the soliton train in the presence of transverse perturbations.

The photonic lattice, however, cannot stabilize every soliton train (even if their amplitude is high). To demonstrate, we consider the soliton trains which bifurcate from the upper edge of the first Bloch band (M -symmetry point) under self-defocusing nonlinearity (with $h = 6$, as before). This soliton family is displayed in Figs. 4(a) and 4(c). From the solution profile shown in Fig. 4(c), we see that the adjacent intensity peaks of these soliton trains are out of phase with each other along both the transverse and longitudinal directions (as is expected since these trains bifurcate from the

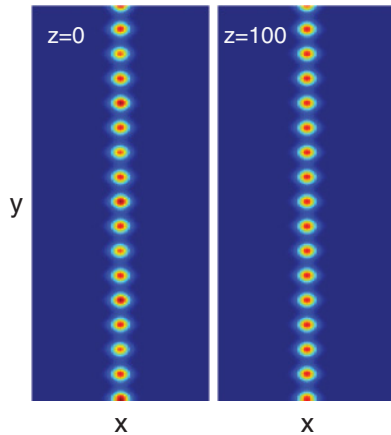


FIG. 3. (Color online) Nonlinear evolution of the soliton train in Fig. 2(c) under 10% initial transverse perturbations (shown are intensity fields $|U|^2$). Left: the initial perturbed soliton train. Right: the solution at $z = 100$.

M -symmetry point). However, this family of soliton trains are all transversely unstable. To demonstrate, the linear-stability spectrum for the high-amplitude soliton train in Fig. 4(c) is shown in Fig. 4(b). The real unstable eigenvalues on the right half of the spectral plane indicate that this high-amplitude soliton train is linearly unstable. The nonlinear instability of this soliton train is displayed in Fig. 4(d). It is seen that, under weak perturbations, this soliton train breaks up into filaments. For this solution family, the transverse instability of low-amplitude soliton trains is neck type (since the diffraction coefficients D_1 and D_2 have the same sign at the M point). Then Fig. 4 shows that the neck-type transverse instability of low-amplitude soliton trains cannot be arrested by the photonic lattice as the soliton train's amplitude becomes high.

From Figs. 2 and 4, we learn that the phase relation of transverse intensity humps also plays an important role

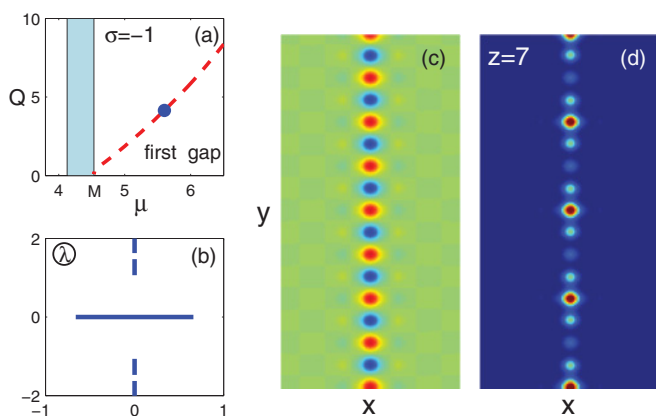


FIG. 4. (Color online) (a) Quasipower curve of the soliton trains bifurcated from the M point of the first Bloch band under self-defocusing nonlinearity (the dashed red line indicates that this whole family is transversely unstable). Panels (b) and (c) show the linear-stability eigenvalue spectrum and profile $u(x,y)$ of the soliton train at the marked point on the quasipower curve ($\mu = 5.6$). (d) Nonlinear evolution ($z = 7$) of the soliton train in (c) under 10% initial transverse perturbations (shown is the intensity field $|U|^2$).

in the stabilization of soliton trains. Specifically, under the defocusing (focusing) nonlinearity, the adjacent transverse intensity peaks of the soliton train should be in phase (out of phase) with each other in order for the train to be stable (as one would expect from dipole stability results [7,25–28]). This requirement on the phase relation translates into a requirement that these soliton trains should bifurcate from the X -symmetry point inside the Bloch band.

We should add that, for the family of soliton trains in Fig. 2, even though they become stable when $\mu > \mu_c \approx 5.44$, if μ gets close to the second Bloch band (whose lower edge is at $\mu = 7.23$), then these soliton trains would become unstable again due to wave coupling to the second band.

IV. TRANSVERSELY STABLE LINE SOLITONS IN THE DISCRETE NLS EQUATION

In the previous section, we demonstrated the existence of transversely stable soliton trains in the continuous lattice model (2.1). In this section, we corroborate this finding by showing that the analogous transversely stable line solitons exist in the discrete NLS model as well. The discrete NLS model is often used to qualitatively describe wave dynamics in the continuous lattice model (2.1) with a deep lattice potential under the tight-binding approximation [28]. In this context, the variable in the discrete model can be viewed as the complex amplitude of the ground-state eigenmode of each lattice-cell potential. The approximation of the continuous model (2.1) by the discrete NLS equation is a significant reduction. Under this reduction, the soliton train shown in Figs. 2(b) and 2(c) in the continuous model becomes a transversely uniform line soliton in the discrete model [see Figs. 5(c) and 5(d) below]. This treatment simplifies both theoretical analysis and numerical computations.

The discrete NLS equation we consider is

$$i \frac{d}{dz} U_{m,n} + \Delta_2 U_{m,n} + \sigma |U_{m,n}|^2 U_{m,n} = 0, \quad (4.1)$$

where Δ_2 is the two-dimensional difference operator:

$$\begin{aligned} \Delta_2 U_{m,n} \equiv & (U_{m+1,n} - 2U_{m,n} + U_{m-1,n}) \\ & + (U_{m,n+1} - 2U_{m,n} + U_{m,n-1}), \end{aligned}$$

and $\sigma = \pm 1$ is the sign of nonlinearity. Here, the intersite-coupling coefficient in front of $\Delta_2 U_{m,n}$ has been normalized to unity through scalings of z and $U_{m,n}$. An important property of this discrete model is that self-focusing and self-defocusing nonlinearities can be transformed to each other since this model is invariant under the transformation [27]

$$U_{m,n} \rightarrow (-1)^{m+n} e^{-8iz} U_{m,n}^*, \quad \sigma \rightarrow -\sigma. \quad (4.2)$$

This transformation is very helpful for us to understand the connection on soliton configurations and their stability properties between self-focusing and self-defocusing nonlinearities. It also means that one only needs to study one type of nonlinearity (say, the self-defocusing nonlinearity) and infer the results for the other type of nonlinearity by this transformation.

Solitons in the discrete model (4.1) are sought in the form

$$U_{m,n}(z) = u_{m,n} e^{-i\mu z}, \quad (4.3)$$

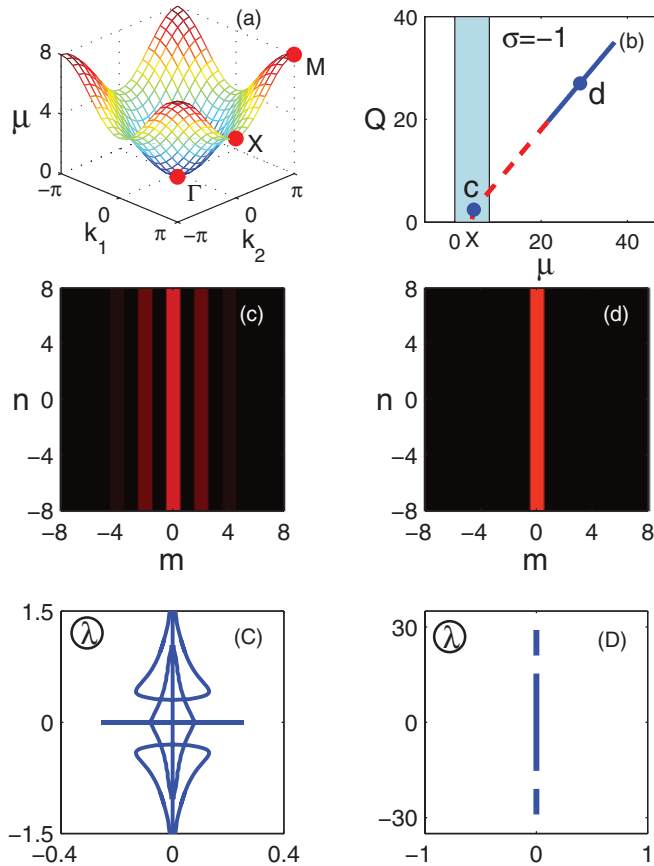


FIG. 5. (Color online) (a) Diffraction surface (4.5) of the discrete NLS equation. (b) Quasipower curve of discrete line solitons bifurcated from the X point inside the continuum band under the self-defocusing nonlinearity; the dashed (red) segment is transversely unstable, while the solid (blue) segment is stable. Panels (c) and (d) show profiles $u_{m,n}$ of discrete line solitons at low and high amplitudes, respectively. These solitons are located at the points marked by the same letters on the quasipower curve of (b). Panels (C) and (D) show linear-stability spectra for the discrete line solitons in (c) and (d), respectively.

where $u_{m,n}$ is a real-valued function which satisfies the equation

$$\Delta_2 u_{m,n} + \mu u_{m,n} + \sigma u_{m,n}^3 = 0, \quad (4.4)$$

and μ is the propagation constant. When $u_{m,n}$ is infinitesimal, the nonlinear term in (4.4) drops out, and the bounded solution to the remaining linear equation is then a discrete Fourier mode, $u_{m,n} = e^{i(k_1 m + k_2 n)}$, where $-\pi \leq k_1, k_2 \leq \pi$ are wave numbers along the m and n directions. Inserting this discrete Fourier mode into the linear part of Eq. (4.4), we get the diffraction relation

$$\mu = 2(2 - \cos k_1 - \cos k_2). \quad (4.5)$$

The corresponding diffraction surface is shown in Fig. 5(a). It is easy to see that this diffraction surface closely resembles the first Bloch band of the continuous model (see Fig. 1). Thus the discrete model (4.1) is appropriate for describing wave dynamics associated with the first Bloch band in the continuous model (2.1). Notice that the continuous spectrum of this discrete model (4.1) contains only a single band

$0 \leq \mu \leq 8$, while the continuous spectrum of the continuous model (2.1) contains multiple Bloch bands. Thus if wave dynamics in the continuous model (2.1) involves higher Bloch bands, the discrete model (4.1) will be inappropriate.

Corresponding to the continuous soliton trains in Fig. 2, we can find a family of discrete line solitons that bifurcate from the X -symmetry point of the continuum band under the self-defocusing nonlinearity ($\sigma = -1$). These discrete line solitons $u_{m,n}$ are n independent, thus they are simply 1D discrete solitons in the 2D model (4.4). These discrete solitons can be computed numerically by the same squared-operator iteration methods or the Newton-conjugate-gradient method in Ref. [7] with very minor modifications. The quasipower curve of this soliton family is shown in Fig. 5(b). Here the quasipower Q is defined as

$$Q(\mu) = \sum_{m=-\infty}^{\infty} u_{m,n}^2. \quad (4.6)$$

Profiles of two typical solitons, near and far from the X point (with $\mu = 4.4$ and 29 respectively), are displayed in Figs. 5(c) and 5(d). The one in Fig. 5(c) has low amplitude (quasipower) and is longitudinally broad, which is the counterpart of the low-amplitude soliton train in Fig. 2(b). The one in Fig. 5(d) has high amplitude (quasipower) and is longitudinally strongly localized, which is the counterpart of the high-amplitude soliton train in Fig. 2(c). To determine the transverse stability of these discrete line solitons, we have computed their linear-stability spectra by the Fourier collocation method [7], and the results are displayed in Figs. 5(C) and 5(D). The spectrum in Fig. 5(C) indicates that the low-amplitude discrete line soliton in Fig. 5(c) is transversely unstable. In addition, this spectrum qualitatively closely resembles the continuous counterpart in Fig. 2(B). The spectrum in Fig. 5(D), on the other hand, does not contain any unstable eigenvalue, indicating that the high-amplitude discrete line soliton in Fig. 5(d) is transversely stable. Thus, the existence of transversely stable discrete line solitons is established. In the present discrete model (4.1), the threshold for transversely stable line solitons is at $\mu > \mu_c \approx 21.5$, or $Q > 39.0$.

Now we examine nonlinear developments of these discrete line solitons under transverse perturbations. We find that, when these solitons are linearly unstable [see Fig. 5(b)] then, under perturbations, they would develop a snake instability and eventually disperse away. This is illustrated in Figs. 6(a) and 6(b) for the low-amplitude discrete line soliton in Fig. 5(c). Analytically, this snake instability can also be understood. Briefly speaking, the envelope of a low-amplitude discrete solution to Eq. (4.1) is governed by an equation similar to (3.2), where D_1 and D_2 are the diffraction coefficients. At the X -symmetry point, $D_1 D_2 < 0$, thus the line soliton to this envelope equation suffers a snake-type instability [1,6,7], which translates into the snake instability observed in Figs. 6(a) and 6(b). When the discrete line solitons are linearly stable [see Fig. 5(b)], however, they would propagate robustly for all distances without breakup. This is illustrated in Figs. 6(c) and 6(d) for the high-amplitude discrete line soliton in Fig. 5(d).

By comparing these results for the discrete NLS model (4.1) to those for the continuous model (2.1), one can easily see that the results for both models are qualitatively almost identical. For both models, we discovered transversely stable

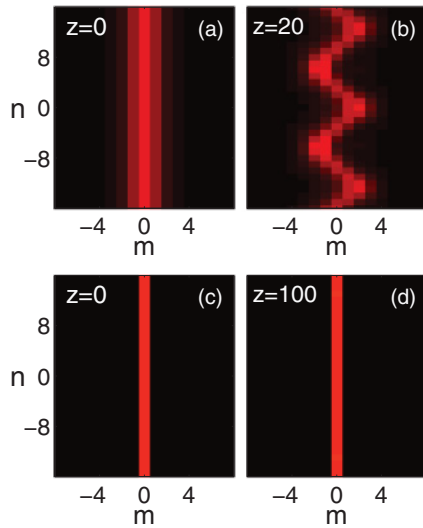


FIG. 6. (Color online) Nonlinear evolutions of discrete line solitons in Figs. 5(c) and 5(d) under 10% initial transverse perturbations (shown are intensity fields $|U|^2$). Upper row: low-amplitude case. Lower row: high-amplitude case.

soliton trains under similar conditions; namely, when they bifurcate from X -symmetry points and have high amplitudes. The instability behaviors for low-amplitude soliton trains are also the same in both models. However, minor differences between the two models do exist. For instance, in the discrete model, line solitons bifurcated from the X point in Fig. 5

are transversely stable for all $\mu > \mu_c \approx 21.5$, while in the continuous model, soliton trains bifurcated from the X point in Fig. 2(a) can become unstable again when μ gets close to the second Bloch band. The reason for this difference is that the discrete model cannot capture the multiband coupling, as we have mentioned earlier in this section.

V. SUMMARY

In summary, we have reported the existence of transversely stable soliton trains in optics. These soliton trains are found in two-dimensional square photonic lattices when they bifurcate from X points (with saddle-shaped diffraction) inside the first Bloch band and their amplitudes are above a certain threshold. These stable soliton trains arise due to the combined effect of the photonic lattice, proper transverse phase relation, and strong longitudinal localization. We have also shown that soliton trains with low amplitudes or bifurcated from edges of the first Bloch band (Γ and M points) still suffer transverse instability. These results have been obtained in both the continuous lattice model and the discrete NLS model, and results from both models are in very good qualitative agreement.

ACKNOWLEDGMENTS

This work is supported in part by the Air Force Office of Scientific Research (Grant USAF 9550-09-1-0228) and the National Science Foundation (Grant DMS-0908167).

- [1] V. E. Zakharov and A. M. Rubenchik, *Sov. Phys. JETP* **38**, 494 (1974).
- [2] N. N. Akhmediev, V. I. Korneev, and R. F. Nabiev, *Opt. Lett.* **17**, 393 (1992).
- [3] A. V. Mamaev, M. Saffman, and A. A. Zozulya, *Europhys. Lett.* **35**, 25 (1996).
- [4] A. De Rossi, S. Trillo, A. V. Buryak, and Y. S. Kivshar, *Phys. Rev. E* **56**, 4959 (1997).
- [5] A. De Rossi, S. Trillo, A. V. Buryak, and Y. S. Kivshar, *Opt. Lett.* **22**, 868 (1997).
- [6] Y. S. Kivshar and D. E. Pelinovsky, *Phys. Rep.* **331**, 117 (2000).
- [7] J. Yang, *Nonlinear Waves in Integrable and Nonintegrable Systems* (SIAM, Philadelphia, 2010).
- [8] S. P. Gorza, Ph. Emplit, and M. Haelterman, *Opt. Lett.* **31**, 1280 (2006).
- [9] A. B. Aceves, C. De Angelis, G. G. Luther, and A. M. Rubenchik, *Opt. Lett.* **19**, 1186 (1994).
- [10] D. Neshev, A. A. Sukhorukov, Y. S. Kivshar, and W. Krolikowski, *Opt. Lett.* **29**, 259 (2004).
- [11] C. Anastassiou, M. Soljacic, M. Segev, E. D. Eugenieva, D. N. Christodoulides, D. Kip, Z. H. Musslimani, and J. P. Torres, *Phys. Rev. Lett.* **85**, 4888 (2000).
- [12] Z. H. Musslimani, M. Segev, A. Nepomnyashchy, and Y. S. Kivshar, *Phys. Rev. E* **60**, R1170 (1999).
- [13] Z. H. Musslimani and J. Yang, *Opt. Lett.* **26**, 1981 (2001).
- [14] B. B. Kadomtsev and V. I. Petviashvili, *Sov. Phys. Dokl.* **15**, 539 (1970).
- [15] V. Zakharov, *JEPT Lett.* **22**, 172 (1975).
- [16] F. Rousset and N. Tzvetkov, *Invent. Math.* **184**, 257 (2011).
- [17] Z. Chen, H. Martin, E. D. Eugenieva, J. Xu, and A. Bezryadina, *Phys. Rev. Lett.* **92**, 143902 (2004).
- [18] C. Lou, X. Wang, J. Xu, Z. Chen, and J. Yang, *Phys. Rev. Lett.* **98**, 213903 (2007).
- [19] X. Wang, Z. Chen, J. Wang, and J. Yang, *Phys. Rev. Lett.* **99**, 243901 (2007).
- [20] O. Morsch and M. K. Oberthaler, *Rev. Mod. Phys.* **78**, 179 (2006).
- [21] M. Skorobogatiy and J. Yang, *Fundamentals of Photonic Crystal Guiding* (Cambridge University Press, Cambridge, 2009).
- [22] Z. Shi and J. Yang, *Phys. Rev. E* **75**, 056602 (2007).
- [23] D. E. Pelinovsky, A. A. Sukhorukov, and Y. S. Kivshar, *Phys. Rev. E* **70**, 036618 (2004).
- [24] G. Hwang, T. R. Akylas, and J. Yang, *Physica D* **240**, 1055 (2011).
- [25] J. Yang, I. Makasyuk, A. Bezryadina, and Z. Chen, *Opt. Lett.* **29**, 1662 (2004).
- [26] L. Tang, C. Lou, X. Wang, D. Song, X. Chen, J. Xu, Z. Chen, H. Susanto, K. Law, and P. G. Kevrekidis, *Opt. Lett.* **32**, 3011 (2007).
- [27] M. Matuszewski, C. R. Rosberg, D. N. Neshev, A. A. Sukhorukov, A. Mitchell, M. Trippenbach, M. W. Austin, W. Krolikowski, and Y. S. Kivshar, *Opt. Express* **14**, 254 (2006).
- [28] P. G. Kevrekidis, *The Discrete Nonlinear Schrödinger Equation* (Springer, Berlin, 2009).
- [29] B. Deconinck, D. E. Pelinovsky, and J. D. Carter, *Proc. R. Soc. A* **462**, 2039 (2006).
- [30] Z. Shi, J. Wang, Z. Chen, and J. Yang, *Phys. Rev. A* **78**, 063812 (2008).